Digest Journal of Nanomaterials and Biostructures Vol. 10, No. 4, October - December 2015, p. 1161 - 1180

SURFACE MELTING AND THERMAL ABLATION PATTERNS INDUCED IN ENAMEL AND CEMENTUM BY 10.6-μm TEA-CO_2 LASER RADIATION. III. THEORETICAL MODELS FOR PLASMA AND SURFACE WAVES EFFECTS

E. A. PREOTEASA[a], I. N. MIHAILESCU[b*], E. S. PREOTEASA[c]
[a]*Horia Hulubei National Institute of Physics and Nuclear Engineering, P.O. Box MG-6, 077125 Bucharest-Magurele, Romania*
[b]*National Institute for the Physics of Lasers, Plasma and Radiation, [P.O. Box MG-36, 077125 Bucharest-Magurele, Romania*
[c]*Helident Ltd. Dental Surgery, Bucharest, Romania*

Further theoretical analysis of the physical interactions between the TEA-CO_2 (10.6μm) laser radiation and dental enamel is reported. The ~2 μs long pulses correspond to the melt expulsion domain where plasma is produced with a high yield by colisional ionization in vaporized substance, even at 1.25 10^7 W/cm^2 only (5 J/pulse and spots of 5 mm diameter). More than half of the incident energy is probably lost in formation of plasma and its screening effects, but returned partly as shock waves or infrared radiation. The shock wave pressure produced by plasma was shown to be inferior to the tensile strength of calcified tissues, and it does not disrupt directly the enamel. Thus the cracks and calcinations beyond the spot boundaries were assigned to radiative heating by plasma. The contribution of the later to these clinically undesired effects appears to be more important than downward and radial heat transfer during and after the laser pulse. Assuming a simple description of the hydrodynamic effects in the liquid layer in the melt expulsion domain, a new model was postulated. The non-resonant as well as the resonant periodic structures (NRPS and RPS) observed in both types of enamel were interpreted in terms of frozen surface capillary and thermal capillary waves of the melted enamel layer. Surface waves were generated by a sudden pressure build-up in the liquid phase at the center of the spot by direct heat generation from the Gaussian profile laser pulse, without plasma involvement. In the 'shallow water' regime, the relative energy fluxes per unit of wave-crest length and the relative total power stored in the wave systems were evaluated. The total stored energy was larger in the enamel with perpendicular prisms (42 μm NRPS + 11 μm RPS) as compared to the one with parallel prisms (68 μm NRPS), in agreement with the larger surface density of defects in the former. If the 42 μm NRPS and the 11 μm RPS are assumed to be thermal capillary waves due to fluctuations only, both modes undergo equipartition and store a mean energy of $kT/2$ each, in agreement to the melt expulsion regime.

(Received August 13, 2015; Accepted October 15, 2015)

Keywords: TEA-CO_2 laser, Dental enamel, Prism orientation,Ablation pattern, Plasma generation, Shock wave pressure, Spot boundaries and halo, Cracks, Radiative heating, Periodic structures, Thermophysical description. Surface capillary waves model, Thermal capillary waves model, Surface density of defects

1. Introduction

Lasers conquested a field of large diversity both in clinical dentistry (reviews in [1 – 3]) and in dental research. In previous work we performed an experimental investigation [4] followed

* Corresponding author: ion.mihailescu@inflpr.ro

by a theoretical study [5], henceforth refered to as Part I and Part II, of the ablation patterns induced in dental enamel and cementum by a pulsed TEA-CO_2 laser (10.6μm). The CO_2 laser applications in dentistry are based mainly on the strong absorption of its infrared radiation by hydroxyapatite from enamel, cementum and dentin. They include among other the surgery of maxilo-facial bones [6], cavity preparation by thermal [7] and hydrokinetic [8] ablation, tooth whitening [9] and activation of teeth bleaching agents [10], and caries prevention by surface modifications of enamel, cementum and dentin. The later type of approach aims to reduce the demineralization by various procedures such as fusion of surface enamel layer for a sealing effect [11 – 14] alone or combined with fluoride application on enamel [15, 16] and on cementum of the root surface [17], and laser fusion of synthetic hydroxyapatite on enamel as a sealant for pits and fissures [18].

Nevertheless, the CO_2 lasers radiation also produces detrimental effects in the hard dental tissues such as cracking, fissuring and disruption of enamel rods, loss of tooth structure [19] and loss of the odontoblastic layer [20]. Research aimed to understand better the mechanisms involved and to reduce these effects is in progres. In fact experimental and theoretical studies are developped in the study of physical interactions of the CO_2 laser radiation with the hard dental tissues [21 – 26]. Models of pulsed laser ablation of enamel and dentine were elaborated to evaluate the light diffusion and distribution, heat transport, temperature distribution and thermal effects in the hard dental tissues caused by the CO_2 laser irradiation of teeth [22]. Most frequently (but with notable exceptions [27, 28]) the models are based in the essence on the diffusion equation [23, 29] which is solved in various approximations, including by Monte Carlo and finite volume methods [30 – 32].

We evidenced by SEM and AFM a large variety of ablation patterns produced by the ~2 μs pulsed TEA-CO_2 laser beam of 10.6 μm in the dental enamel at 75, 175 and 625 J/cm^2 nominal fluence (Part I [4]). Complex ultrastructural changes were evidenced in the spot, at the boundary and beyond the boundary. In general, the laser-induced changes were dependent on the orientation of the enamel prisms with respect to the surface. In Part II [5] we approached the theoretical interpretation of ablation mechanisms emphasizing physical concepts more close to experiment as compared to the models mentioned above; we follow the same philosophy here.

The analysis carried on in Part II [5] of the surface roughness vs. fluence relationship determined by AFM on the laser-irradiated enamel with perpendicular prisms, showing a fluence threshold and asymptotic saturation, evidenced the competition between the laser pulse melting of the surface layer and a ‘relaxation’ by own internal dynamics with an energy barrier, formally similar not only to other laser ablation effects but also to absorption-desorption phenomena.

Nevertheless, the most striking effects were evidenced by SEM in the laser spot and consisted in the formation of resonant periodic structures (RPS) of ~11 μm wavelength in enamel with perpendicular prisms, and of concentric nonresonant periodic structures (NRPS) of ~42 μm periods in the enamel with perpendicular prisms and of ~68 μm in the enamel with parallel prisms [4]. The formation of RPS, first observed by us in dental enamel is also, to our knowledge, the first such effect evidenced in biological materials in general. Therefore we focused on the mechanisms underlying the formation of RPS in Part II of this study [5] by referring both to the electrodynamic and to the thermophysical current theories (review in [33]). Noteworthy, the theoretical predictions of the electrodynamic model of diffraction and interference of laser radiation in the melted surface layer [33] fit excellently to the ~11 μm RPS observed in enamel [5]. However, neither of the two descriptions of RPS could be applied also to the formation of NRPS. Implicitly, the dependence of NRPS period on the orientation of the enamel prisms was not addressed in Part II [5]. In general there are few theoretical studies which account for the heterogeneity [34] and the anisotropy [35] of biological tissues in explaining the laser action effects. On this line one remarkable investigation assumes a heterogeneous structure of enamel and analyses the role of pore and layer water at nm and μm scales for stress generation in enamel ablated with CO_2 (at 10.6 μm) and Er:YAG lasers (at 2.94 μm) [36]. Given the important questions on NRPS remained unanswered in Part II, we propose here a novel theoretical approach of the ablation pattern in terms of frozen surface capillary waves and thermal capillary waves of the melted enamel layer. This endeavor is

aimed chiefly to the understanding of NRPS formation and of their dependence on prism orientation; but its relevance to RPS formation is considered also in view of a new perspective.

Other effects associated to the laser ablation will be discussed in addition, includind the ultrastructural configurations observed in enamel at the spot boundary and their dependence on the prisms orientation, thermal damage of the enamel area outside the crater and splashing of molten enamel or debris beyond the spot boundary.

A particularly important role in the generation of the above ablation patterns and side effects in enamel could be due to plasma-associated phenomena such as radiative thermal damage, shock and acoustic waves. This is because the TEA-CO2 laser is known for the large losses from the incident energy in the formation of plasma, and because a significant part of the plasma energy is returned by the mentioned processes. Therefore the place of plasma generation in the energy balance and in the time evolution of the laser pulse will be discussed in relation to heat diffusion and to the ablation patterns inside the spot, at its boundary and beyond.

To resume, the aim of Part III remains, hereafter as much as in Part II [5], a better understanding of the mechanisms underlying the ablation patterns produced in enamel by the TEA-CO_2 laser irradiation, by a theoretical analysis based on experimentally oriented physical concepts. A new model of frozen surface capillary waves and thermal capillary waves of the melted enamel layer is proposed to explain the periodic structures and their dependence on prisms orientation. The processes involved in plasma generation and in plasma-associated phenomena with modulatory effects on the ablation patterns are discussed.

2. Physical mechanisms and models of plasma and surface waves effects

General survey

The particular ultrastructure characteristics of the ablation patterns visible in the dental enamel irradiated with the pulsed TEA-CO_2 laser express the parameters of laser radiation and the response of the material. For good reason, one can suppose that significantly different characteristics of the laser radiation parameters would result in different ablation patterns of the same material. Different physical domains of beam–matter interaction can be defined and classified according to the pulse parameters. In a recent review [37], the most important laser pulse parameters are considered: photon energy, intensity [W/cm^2], pulse duration, and beam spot radius; let apart pulse duration which is essential to any perspective, they obviously define alternatively the more popular parameters of wavelength, pulse and total applied fluence [J/cm^2], and spot diameter or spot surface. In our experiments: λ = 10.6 μm ($h\nu$ = 0.117 eV), t_L = 2 μs, ϕ_{spot} = 0.5 cm, Φ_{pulse} = 25 J/cm^2, I = 1.25 x 10^7 W/cm^2. In addition, the beam profile was Gaussian and the radiation was unpolarized. With certain of these values we can place our case in a general frame.

According to the pulse duration, the domains of “cold ablation” (fs pulses), “hot ablation” (ps pulses) and “melt expulsion” (ns to μs pulses) are differentiated [37]. The long pulse duration of 2 μs of the TEA-CO_2 laser clearly corresponds to the melt expulsion domain. In fact, in Part I [4] we showed by SEM that turbulent boiling produced splashing of microscopic melted enamel droplets. The melt flow is limited by inertia being characterized by a time t_{in} and by friction of the liquid at the solid melting front. Various time constants are well separated on time scale (melting time, t_m ~ 0.1 μs; relaxation time of the melt flow, t_{relax} ~ 1 – 10 μs; the time the flow takes for moving in the ablated spot, t_l ~100 μs), and this allows for the development of relatively simple models [37]. The radiation also interacts with the ablated material in the plasma.

By another classification criterion, intensities below 10^{11} W/cm^2 define the „heating” domain [37], to which our experiments belongs with ~10^7 W/cm^2 per pulse. This domain, typical for ablation microprocessing regime, is characterized by the collisional excitation and ionization in vapors which dominate the formation of ionized plasma. The phenomena are simpler than at intensities above 10^{11}W/cm^2 where multiphoton interactions, field and tunnel ionisation and

nonlinear atomic effects dominate. and can be described by thermodynamics and continuum physics.

This brief discussion shows that in our ablation experiment with μs-long pulses, plasma generation and hydrodynamic effects in melted enamel could be understood in a simple physical picture without unnecessary complications. This is what we attempted to do in our models.

Plasma generation:

The most important loss of energy from the TEA-CO_2 laser beam is due to plasma formation in the vapor plume mainly by collisional ionization. Due to the relatively long pulse duration of ~2 μs, the domain of melt expulsion is characterized by the lowest values not only for the ablation threshold but also for the thresholds of plasma generation and radiation absorption in plasma; these three parameters increase monotonously for shorter laser pulse durations [37]. The TEA-CO_2 laser radiation is characterized by high plasma induction with an important role in ablation [38 – 40], and dental applications are not excepted [10]. Other lasers with short pulses were used just for plasma ablation of hard dental tissues [24]. In addition to losses, we previously mentioned that plasma formation could be involved in the observed alteration of enamel and contribute to the generation of the concentric periodic patterns, of the halo outside the laser spot and possibly to the roughness growth of irradiated surfaces.

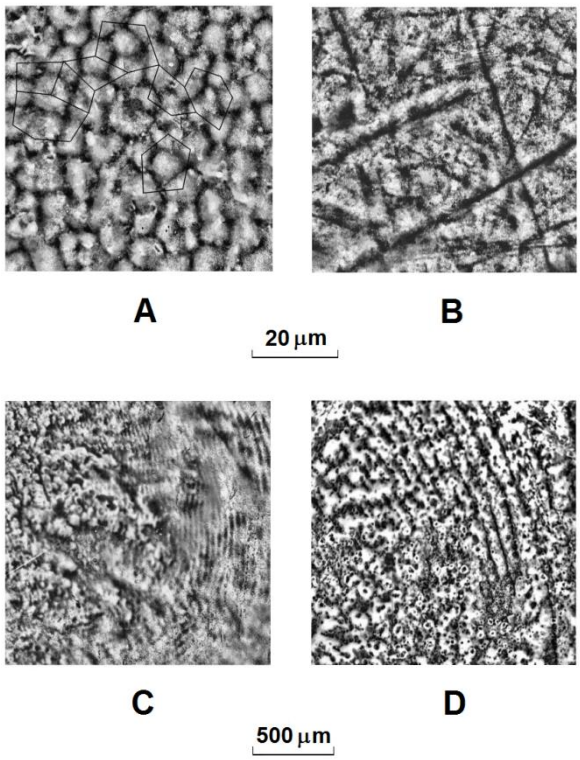

Fig. 1. –Native enamel (A, B) and ablation patterns of enamel (C, D) after irradiation with a 625 J/cm^2 fluence (25 pulses). A, C – lower molar with perpendicular prisms. B, D – upper incisor with parallel prisms. Non-resonant periodic structures directed to the exterior of the spots and violent boiling in the central areas are seen. The periods of the non-resonant waves were of about 42 μm in the enamel with perpendicular prisms (C) and of about 68 μm in the enamel with parallel prisms (D).

In air, the dielectric breakdown takes place above a surface density of power of about 10^{11} W/cm^2. For the 5 J pulses produced by the pulsed CO_2 laser, this threshold is reached in air and a spark was produced when the radiation was focused freely to a diameter of 50 μm only. Thus with the beam focused to a spot of 5 mm on the tooth specimen surface, air breakdown could

not contribute by itself to the incandescent plume. However, air breakdown and plasma formation by laser irradiation is strongly facilitated near a solid target by vapor production [40 – 43]. Plasma formation was therefore mainly due to vaporized atoms from the enamel itself. Moreover, the threshold for the plasma onset is lowered by surface defects [38, 41]; in fact, the enamel surface contains a significant density of defects (Fig. 1A and 1B; Table 1 of Part I [4]).

The estimation of the mean energy density per single pulse absorbed in enamel which produced the plasma from vaporized enamel, depends on the assumed thickness of the laser thermally-affected layer. Assuming a thickness of 20 – 40 μm, equal to the penetration depth $\delta = d = 1/\mu_a$ estimated in Part II [5], one finds 6400 - 12700 J/cm^3; for $\delta = z_{99} = 90 – 180$ μm representing the depth where 99% of the non-reflected and non-scattered radiation is absorbed, the result is 1600 – 3200 J/cm^3. A reasonable value could be the geometric mean of these values, namely 3200 – 6400 J/cm^3 for the energy density per single pulse absorbed in enamel. This value correlates well to a threshold of 3100 J/cm^3 found for the plasma formation by 10.6 μm irradiation of skin [44]. The irradiance at the enamel surface was of the order of 10^7 W/cm^2, close to the plasma ignition threshold of 10^8 W/cm^2 in soft biological tissues [44, 45]. The lower threshold in enamel may be attributed to its surface defects. For plasma mediated ablation produced by ultrashort 50 fs laser pulses generated using a Ti:sapphire chirp modulation pulse amplifier system with a frequency-doubled, Nd:YAG pump laser, the plasma formation fluence threshold for both enamel and dentin was 0.4 J/cm^2 [24]. Although our pulse parameters were different of these authors, the plasma formation threshold was undoubtfully lower than the rather high fluence of 25 J/cm^2 used per pulse, explaining therefore the observed breakdown.

Plasma generation played an important role in the energy balance. Due to the relatively long duration of the laser pulse (~2 μs) with respect to the plasma generation time (~150 ns), the radiation interacts with the ablated material in the gaseous plasma phase and the IR opaque plasma screened the rest of incident radiation and prevented it to reach the dental specimen surface. This resulted probably in losses as large as 50 – 70 % of the absorbed energy. Thus while the 3, 5 and 25 applied pulses delivered a 'nominal' fluence of 75, 175 and 625 J/cm^2, by taking into account the plasma formation and the other losses, the approximate 'effective' fluence involved in the ablation processes ,which changed the surface (ultra)structure could be, supposedly, of only 25 ± 12, 60 ± 28and 212 ± 100 J/cm^2. These values could be useful for a possible comparison to the ablation characteristics produced with very short pulse (fs) lasers, which do not lose much energy by plasma production in the "cold ablation" regime [37]. However, the effective fluence due to absorbed radiation energy in enamel depends in an unknown way on the orientation of enamel prisms.*

Part of the plasma energy returned in the form of shock and acoustic waves and of radiative heating of the enamel. Due to the Gaussian profile laser pulse, a temperature significantly higher than 1600 ^{o}C was undoubtfully reached in the center of melted enamel, leading to induction of boiling enamel bubbles (Fig. 1C and 1D), as already mentioned. Such a strong heating is also expected due to the high temperature of plasma: the temperature color in the plasma of lased teeth is of 2700 – 3000 ^{o}C [46]. In any case, the estimated heating rate of the enamel could be of the order of 10^8 Ks^{-1}, consistent to an ensemble of highly turbulent process resulting in the observed surface morphology changes. In the melt expulsion domain of μs-long pulses, nonlinear transport phenomena, e.g. turbulence, due to the fast movement of the ablation front occur [37].

The fast heating causes the spherical expansion of plasma to generate shock and acoustic waves in the specimen and air. The later exert pressure on the molten layer of solid targets [47, 48] and of the enamel in particular, being able to induce outside radial transport of fluidized material. In fact the pressure P_M exerted on the target by the shock waves produced by the plasma expansion

*The effective fluence incertitude was estimated based upon the assumption of independent action of the successive pulses and thus, by error propagation formula, $\varepsilon = \varepsilon_o N^{1/2}$ where ε_o is the error in the evaluation of fluence delivered by a single pulse and N is the number of applied pulses. This argument applies in part also to the standard deviation of the RMS roughness R (Fig. 1 of Part II) which increases with the fluence, probably due to plasma formation which is a less controllable phenomenon. Such a behavior of the errors was observed for the effects of CO_2 laser irradiation on dermis and was attributed to plasma formation [44].

may be higher than the tensile strength of many materials. Expressed in Mbar, the shock wave plasma pulse pressure is given by the formula [49]:

$$P_M = 12.3 \left(\frac{I_L}{10^{14}}\right)^{\frac{2}{3}} \lambda^{-\frac{2}{3}} \left(\frac{A}{2Z}\right)^{\frac{1}{3}} \quad (1)$$

where I_L is the pulsed laser intensity in W/cm^2, λ the wavelength of the laser photons in μm, *A* the atomic weight and *Z* the atomic number of the irradiated target (quoted in [50]). This formula suggests the elemental composition of the target and thus of elemental analysis by various methods (XRS, IBA and LIBS) to be significant of for understanding the effects of plasma shock wave. However, except for hydrogen (where A/2Z ~ 0.5), for all elements A/2Z ~ 1. With our experimental values (I = 1.25 10^7 W/cm^2, λ = 10.6 μm) we get for the shock wave of plasma pulse a pressure P_M = 6.4 10^{-5} Mbar = 6.4 MPa (approx. 62 atm), which is appreciable but much lower than the tensile strength of bone (100 – 130 MPa) and so much the more than that of the enamel. Therefore, for the used irradiance the plasma shock wave induced by the pulsed TEA-CO_2 laser does not disrupt the solid enamel and thus it is probably not involved in the formation of cracks, although it may influence the ablation pattern imprinted in the liquid melt.

The shock wave mechanism may play a role in imprinting the ablation patterns observed at the highest nominal fluence applied on enamel (625 J/cm^2). This way, a fraction of the energy lost in vaporization and plasma generation and heating is returned and used for the modeling of the tooth surfaces. A thermo-acoustical-mechanical effect could account for the splashing of molten enamel or flaked-of debris beyond the spot boundary (Fig. 7C and 7D of Part I [4]). It is also plausible that the pressure of the shock and acoustic waves attained its maximum at the center of the spot and, acting on the molted enamel layer, contributes to generate the concentric NRPS waves expanding towards the periphery (Fig. 1C an 1D). This image is consistent with the fact that the density of the plasma reaches its highest value at the center of the spot and decreases rather abruptly at margins [41]. Therefore the plasma could be expected to produce the strongest heating and pressure at the center of the spot and thereby, to induce here, the turbulent boiling of the enamel with subsequent radial dissipation of energy in the form of concentric waves. As pointed out in Parts I and II, plasma action may also contribute to the AFM-observed enamel roughness vs. fluence relationship which is depending on the fluence effects in the generation of plasma on metallic targets [41] (as well as with other effects in laser ablation). Nevertheless, the significance of the mentioned similarity is still unclear and further confirmation is needed.

The heat transfer from plasma to the surroundings of the irradiation spot, most probably by radiation, could explain at least in part, the ultrastructure of the spot boundary, the splashing of enamel debris beyond the spot boundary and the thermally damaged (calcined) area of enamel outside the crater, which will be discussed further (see Fig. 4a); this does not exclude a possible contribution to the damage to be produced by the slower heat diffusion from the melted enamel (see below).

Simple physical model of concentric nonresonant waves generated by thermo-mechanical effects. Surface waves' model:

One of the remarkable results in Part II [5] was the excellent agreement between the theoretical predictions for resonant periodic structures based upon the electrodynamical mechanism of diffraction and interference of laser radiation in the melted surface enamel layer ($\langle\Lambda\rangle_{theor}$ = 11.13 ± 0.14 μm) and the experimental value measured by SEM (Λ_{e} = 11.0 ± 1.5 μm). A diversity of electrodynamic mechanisms for RPS formation was proposed in the literature (review in [33]). We consider our results remarkable as we used long duration pulses (~2 μs) of unpolarized radiation, while recent advances have been achieved both in experiment and theory by use of double-fs-laser-polarized-pulse irradiation sequences (review in [51]). On the other hand the theory did not explain why the RPS formed only in enamel with perpendicular prisms and cannot be extended to the formation of non-resonant periodic structures with periods dependent on the orientation of the enamel prisms. We will now try to understand the NRPS formation by a different approach.

Direct heat generation in enamel inducing the thermo-mechanical changes in surface structure without plasma involvement should be considered among the most important mechanisms of laser action. We observed the most pregnant effects produced after 25 pulses, but they should be considered as additive or cooperative results of the morphological changes brought about by thermally-separated single pulses, because the large time interval between them (10 – 12 sec) allowed complete cooling of enamel. We therefore analyzed the action of single pulses. Next, we refer to SEM images of the enamel irradiated with 25 pulses.

We postulate that thermo-acoustical-mechanical effects due to feed-back of plasma formation could be neglected and primary thermo-mechanical effects could play an important role in the generation of the periodic patterns visible in the peripheric region of the spot, as frozen circular waves. A plausible hypothesis is that the intense irradiation in the center of the spot induced turbulent boiling, vaporization and ejection of the molten enamel, which, by recoil momentum, exerted a sudden pressure build-up on the liquid phase, generating thus the surface waves observed by SEM (Fig. 1C and 1D). This phenomenon occurs in the frame of fully developed melt flow, which is limited by inertia and governed by the equilibrium between the recoil pressure and friction of the liquid at the solid melting front [37]. We therefore propose a simplified surface wave model in order to describe the different characteristics of the periodic patterns in the two types of enamel. One should consider some basic theory which is beyond the scope of our study [52, 53]. Surface waves are described by systems of partial derivatives equations, such as the Boussinesq equations and the 'shallow water equations'. One assumes here a few realistic approximations, in order to compare the two NRPS cases of ~42 and ~68 μm periods Λ generated in the enamel with perpendicular (⊥) and parallel (∥) prisms, respectively. Their phase velocity c_p is defined, as:

$$c_p = \frac{\omega}{k} \tag{2}$$

where $\omega = 2\pi\nu$ and $k = 2\pi/\Lambda$. We assume to be in the 'shallow water' regime, with a depth η of the melted (liquid) enamel layer significantly smaller than the wavelength Λ of the periodic patterns.

$$\frac{\eta}{\Lambda} \ll 1 \tag{3}$$

This condition is valid within large limits, from $\eta/\Lambda < 0.05$ to $\eta/\Lambda < 0.5$ [53, 54]. Probably, our case corresponds to an intermediate depth, which however could still be approximated by the 'shallow water equations'. For the sake of simplicity, we assume to be in the 'shallow water' case; for instance we consider a depth η of the melted enamel layer of 5 – 10 μm, thus smaller enough than Λ. Note that the depth of the melted/liquid enamel layer η is different of the relief depth h which applies to RPS, and also that $h = 1.6$ μm $< \eta = 5 – 10$ μm. This implies the group velocity c_g – namely the speed of the observed waves – to be approximately equal to c_p [54]:

$$c_g \approx c_p = \frac{\omega}{k} \tag{4}$$

The angular frequency ω is related to the wave vector k by the dispersion relation. For the ocean surface waves, the latter is composed of a gravitational and a capillary term. Nevertheless, gravity effects during the very short duration of the laser pulse and, at the scale of tens of micrometers are negligible. Thus, the dynamics of the surface waves produced by the laser pulse in the melted enamel is determined by surface tension only, and the SEM observed periodic patterns are postulated to be frozen, proper capillary waves. Accordingly, the dispersion relation depends on the superficial tension σ, on the density ρ of melted enamel and on the liquid depth η only [55, 56]:

$$\omega^2 \approx \frac{\sigma}{\rho} k^3 \tanh k\eta \tag{5}$$

and hence:

$$c_g \approx \left(\frac{2\pi\sigma}{\rho\Lambda} \tanh k\eta\right)^{\frac{1}{2}} \tag{6}$$

This allows for the evaluation of the speed ratio corresponding to the two values of Λ, $c_{g\perp}$(42 μm)/$c_{g\parallel}$(68 μm). Assuming η = 5 μm in both cases, we get $c_{g\perp}$(42 μm)/$c_{g\parallel}$(68 μm) = 1.54. One may presume that heat propagated deeper along the prisms in the surface layer of the enamel with perpendicular prisms, because in the enamel with parallel prisms the later are in poor thermal contact with each other, and the more disordered mixture of hydroxyapatite crystals and proteins between them are thermoinsulating. Thus, taking η = 10 μm for Λ = 42 μm and η = 5 μm for Λ = 68 μm, the resulting ratio is 1.85. This indicates that in either hypothesis the shorter wavelength NRPS radial waves propagated faster in the enamel with perpendicular prisms (Fig. 1A and 1C).

Another useful relation concerns the energy flux per unit of wave-crest length:

$$\mathcal{P} \sim \rho H^2 c_g \tag{7}$$

where H is the significant wave height. The SEM images of the NRPS show that H is approximately proportional to Λ by a constant quoted q:

$$H \approx q\Lambda \tag{8}$$

where we can take $q \approx 0.75$. As compared to the RPS where H could not exceed $2h$ = 3.2 μm for hydroxyapatite, the q value in the case of NRPS is rather high; so that one could choose a lower q of, say, ~0.30 or less. Nevertheless, the q value is not critical in the following, because only the ratios of various amounts will be evaluated. We have therefore,

$$\mathcal{P} \sim \rho q^2\Lambda^2 c_g \tag{9}$$

and one can evaluate the ratio of the energy fluxes per unit of wave-crest length $\mathcal{P}$ corresponding to the two wavelengths. Thus, $\mathcal{P}_\perp$(42 μm)/$\mathcal{P}_\parallel$(68 μm) is found to be ~0.6 if η = 5 μm in both types of enamel and, respectively, ~0.7 if we assume η = 10 μm in the enamel with perpendicular prisms and η = 5 μm in the enamel with parallel prisms. In brief, the energy flux per unit of wave-crest length is higher in the enamel with parallel prisms (Fig. 1B and 1D).

We can seek for an explanation for the increased period of waves towards the spot periphery. In this zone, the intensity of the beam with an approximately Gaussian ($1/e^2$) profile decreases fast and so does the depth η of melted enamel. Therefore, the height H of the wave increased and presumably the proportionality between H and Λ (eq. 8) no more holds true. At the same time, the energy flux per unit of wave-crest length $\mathcal{P} \sim H^2 c_g$ (eq. 7) keeps constant by virtue of energy conservation and, because $c_g \sim 1/\Lambda^{1/2}$ (eq. 6), the wavelength increased.

Finally, we may evaluate the total energy flux in the whole system of waves, assuming for simplicity, that they occupy the whole spot without turbulence at the center. In general, the energy of the distorted surface of the liquid enamel is:

$$E \approx \frac{\sigma}{2}\int dx\, dy \left[\left(\frac{dH}{dx}\right)^2 + \left(\frac{dH}{dy}\right)^2\right] \tag{10}$$

It cannot be however calculated because the surface landscape H(x, y) could not be determined from standard SEM images. Thus, it will be estimated by the capillary wave approximation that the spot of radius R accommodates Int(R/Λ) concentric wave-crests, totalizing a length of:

$$L = 2\pi\Lambda\left(1 + 2 + \cdots + \mathrm{Int}\frac{R}{\Lambda}\right) = \pi\Lambda\,\mathrm{Int}\frac{R}{\Lambda}\left(1 + \mathrm{Int}\frac{R}{\Lambda}\right) \tag{11}$$

Accordingly, the total power stored in the wave system produced by the laser pulse in the melted enamel is:

$$P = \mathcal{P}L \approx \rho q^2 \Lambda^3 c_g \pi\,\mathrm{Int}\frac{R}{\Lambda}\left(1 + \mathrm{Int}\frac{R}{\Lambda}\right) \tag{12}$$

By substitutions in this formula, one can find for the ratio $\mathcal{P}_\perp$(42 μm)/ $\mathcal{P}_\parallel$(68 μm) the following values: 1.0 if η = 5 μm in both types of enamel; and 1.2, respectively, if η = 10 μm in the enamel with perpendicular prisms and η = 5 μm for parallel prisms. In other words, the energy stored in the two wave systems was about the same or very close irrespective of the prisms' orientation, although the resulting periodic patterns are different (Fig. 1). The same trends for the relative group velocity, the energy flux per unit of wave-crest length and the total energy flux in the whole systems of waves keeps valid when larger depths of the melted enamel layer are postulated (e.g., η = 20 or 30 μm).

If the short wavelength ($\Lambda \approx 11$ μm) RPS in the enamel with perpendicular prisms are considered, we see that the condition of shallow water $\eta/\Lambda < 0.5$ is satisfied only if η = 5 μm is assumed. Taking into account the morphology of the RPS in the ablation pattern (Fig. 4a; and Fig. 3 of Part II [5]) and estimating the total length of the wave-crests, the following results are obtained: for the relative velocity, $c_{g\perp}$(11 μm)/$c_{g\perp}$(42 μm) = 2.45; for the energy flux per unit of wave-crest length $\mathcal{P}_\perp$(11 μm)/$\mathcal{P}_\perp$(42 μm) = 0.97; and $\mathcal{P}_\perp$(11 μm)/ $\mathcal{P}_\perp$(42 μm) = 0.64. The last results also show that the total energy in the RPS plus NRPS wave systems of the enamel with perpendicular prisms is larger as compared to that of the NRPS in the enamel with parallel prisms:

$$\frac{P_\perp}{P_\parallel} = \frac{P_\perp(42\ \mu m) + P_\perp(11\ \mu m)}{P_\parallel(68\ \mu m)} = 1.6 \tag{13}$$

It follows that, the former stores more energy than the later. This is consistent with the much larger surface density of defects in the enamel with perpendicular prisms, which favors the absorption of laser radiation. In fact, as compared to the enamel with parallel prisms, the enamel with perpendicular prisms shows a surface defects density orders of magnitude higher (~$4{\cdot}10^3$ times for point-centered defects and ~50 times for filiform defects [Part I]). Implicitly, it is plausible that the thickness η of melted enamel is larger in the case of perpendicular prisms.

Moreover, in the enamel with perpendicular prisms we note that $\mathcal{P}_\perp$(11 μm) is of the same order of magnitude as $\mathcal{P}_\perp$(42 μm) and even very close to it (within the assumed approximations 0.6 matches roughly to 1.0). This aspect suggests that from a thermo-physical viewpoint the NRPS and the superimposed RPS may have a common origin, notwithstanding the fact that the later are initiated by electrodynamic mechanisms while the former are due only to thermo-mechanical effects. It

seems that in both cases we deal with thermal capillary waves, that is, the surface is distorted by thermal fluctuations [56, 57]. Note that in this case the energy of the wave mode is proportional to H^2, as assumed above for the 'shallow water' surface wave model. Also, both modes undergo equipartition and store a mean energy of $kT/2$. Indeed, for infrared radiation laser pulses with intensities lower than 10^{11}Wcm^{-2} and durations greater than 10 ps, as used in the enamel ablation, the energy is dissipated in local thermal equilibrium [37].

The semiquantitative model of surface waves discussed above, although based on several approximations, leads to some significant results and contributes to a better understanding of the periodic patterns' origins generated by laser radiation in enamel. This is consistent with a picture of the melted enamel layer having a smaller depth (about 5 – 30 μm) as compared to the depth of ~100 μm where 99% of the absorbed radiation energy is deposited in the enamel. This view is consistent to the exponential attenuation of radiation. In particular, the depth of 30 μm corresponds to the penetration depth d where the beam intensity is reduced to 37% from its initial value; the heating produced by this intensity in the deeper layers ~70 μm thick probably induces calcinations and chemical alteration of enamel, but without complete melting. In addition, the depth of melted layer in the two types of enamel may be roughly equal, or possibly larger in the case of the enamel with perpendicular prisms. The observed periodic patterns of Λ ~42 and ~68 μm periods may be physically assigned to frozen capillary waves in the 'shallow water' regime. Moreover, in the enamel with perpendicular prisms the ~42 μm waves propagates faster and stored less energy per unit of wave-crest length as compared to the ~68 μm waves in the enamel with parallel prisms, while the total energy stored in the two surface wave NRPS systems was almost the same regardless of the different orientation of prisms. However, in the enamel with perpendicular prisms the superimposed system of ~11 μm short length RPS waves – which could be thermal capillary waves produced by thermal fluctuations described by electrodynamical mechanisms – stored a total energy almost equal to that of the ~42 μm proper NRPS capillary waves. The energy of the two superimposed wave systems in the enamel with perpendicular prisms amounted therefore to about twice that of the single wave system in the enamel with parallel prisms, in agreement with the higher radiation absorption postulated in the former due to the larger density of surface defects.

Other thermo-mechanical effects

Other mechanisms may also contribute to the generation of wave systems. The very fast local heating with strong lateral and transversal gradients induces an equally fast local dilatation of the melted substance resulting in the oscillatory pattern formation discussed above. However, in this case, the wave systems could be modulated by a far-from-equilibrium phenomenon [58] of turbulence wave type. In fact, a mechanism similar to the Rayleigh-Benard effect – the spontaneous development of a regular pattern of convection cells at the surface of a liquid under certain conditions of heat flow and temperature gradient – was proposed for the laser-induced formation of two-dimensional periodic structures [59].

Ultrastructure of melted enamel in the spot

In connection to the above, brief complements to some aspects discussed in Part I will be made here and in the next subsection. In addition to the dependence of the periodic structures on the orientation of enamel prisms, the ablation patterns showed other ultrastructural differences in the enamel with perpendicular and parallel prisms. The former showed a 'glassy ruggedness' aspect (Fig. 2A), while the glassy appearance of the second was more 'smooth' with narrow fissures (< 1 μm) due to fast solidification (Fig. 2B). The 'glassy ruggedness' of the perpendicular prisms enamel suggests a turbulent boiling and/or a higher temperature. The 'smooth' and glassy enamel with parallel prisms may be due to a complete melting and/or a lower temperature. Also, the diameter of bubbles in the center of the spot was smaller in the enamel with perpendicular prisms as compared to the enamel with parallel prisms (Fig. 1).

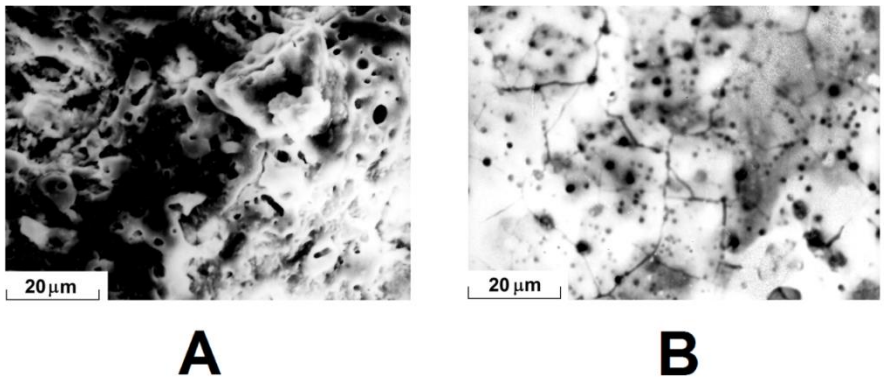

Fig. 2. SEM images at ×2000 magnification of enamel with perpendicular (A) and parallel prisms (B) irradiated at 625 J/cm^2 fluence. The prism heads were completely melted and the fused substance mass was quickly resolidified in an irregular landscape testifying of a more violent boiling in the enamel with perpendicular prisms (A) as compared to theparallel prisms case (B).

One can only speculate that, due to the anisotropic structure, the thermal diffusivity was higher along the prisms than transversally. Given the Gaussian profile of the beam, this resulted in a higher lateral heat diffusion in the enamel with parallel prisms leading to a more uniform local melting, in contrast to the enamel with perpendicular prisms where the lateral propagation of heat was lower, leading to a stronger lateral temperature gradient. This gradient implies a higher turbulence producing the 'glassy ruggedness'. At the same time, the postulated lower transversal thermal diffusivity of the prisms suggests that in the enamel with parallel prisms a thinner layer melted and a higher energy density occurres in the liquid substance at the center of the spot. This could explain the larger diameter of bubbles in the center of the spot with parallel prisms (Fig. 1). The narrow fissures due to fast contraction of enamel observed in the 'smooth' enamel with parallel prisms (Fig. 2B) but not in the enamel with perpendicular prisms (Fig. 2A) suggest a faster heat loss after laser irradiation in the first case, which is also consistent with a smaller thickness of the melted enamel layer. However, it seems that a model of these very complex processes would require arbitrary parameters. Further studies are necessary to understand in detail the observed patterns – including the possible fractal-type structure of the surface [60] as noted in Part I [4] – and their dependence on the enamel prisms orientation.

On the other hand at low fluence (75 J/cm^2) the ablation pattern of the enamel with perpendicular prisms from the upper incisor is comparatively simpler. It shows mostly incipient melting of prisms' heads and limited areas of complete melting with continuous fusion of prisms heads and glassy aspect (Fig. 3).

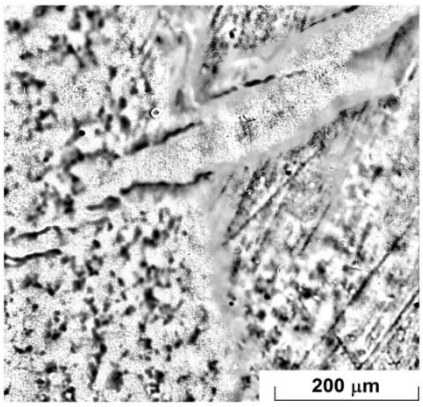

Fig. 3. Ablation pattern of the enamel with perpendicular prisms from the upper incisor irradiated at 75 J/cm^2 nominal fluence. Most prisms heads were incipiently melted; a few areas show complete melting with continuous fusion of prisms heads.

Spot boundary

The large bubbles at the spot center of the enamel with parallel prisms of the wisdom tooth evidence a violent boiling with evaporation and melt expulsion by vapor recoil momentum. This could splash outward some liquid material. At the boundary of the spot and slightly beyond it, the splashed liquid cools down and solidifies fast enough to preserve its characteristic structure with the aspect of a foam or a conglomerate (Fig. 7C and 7D of Part I). The lack of substance splashing or blowing out in the case of perpendicular prisms (Fig. 7A and 7B of Part I) could be explained perhaps by a lower energy density in a deeper melted enamel layer, or by the different orientation of the hydroxyapatite crystals.

Note that the enamel ablated at the intermediate fluence of 175 J/cm^2 (7 pulses) shows an aspect similar to the margin of the spot produced at 625 J/cm^2 (Fig. 3C and 7D of Part I). Therefore, a similar mechanism may be suggested. Exfoliated semi-melted hydroxyapatite crystals – or some melted enamel drops – were splashed and semi-solidified during flight, before adhering to the surface. Similar effects were produced by laser irradiation of a polymer film [61]. However, the origin of the patterns at the boundaries and their dependence on the prisms' orientation requires further investigation.

The calcination halo beyond the spot boundary

The discussion of other thermal effects may be relevant for understanding certain particular observations of indirect laser action, such as the calcination of enamel observed beyond the boundary of the spot at 625 J/cm^2 fluence, and which is virtually absent at 75 J/cm^2 (Fig. 4a and 4c). Similarly, a halo of about 100 μm wide surrounding the spot in laser-irradiated enamel was observed [62]. This outer calcinated area shows two specific features (Fig. 4a): large (5 – 7 μm) fissures at 50 – 100 μm apart of each other, and superficial melting of the prisms' heads accompanied by their incipient fusion, at least up to distances of about 300 μm from the spot boundary (and probably also beyond the margin of the SEM image). Incipient prisms' melting has been also observed by other groups [63]. Note that the short-wavelength RPS pattern produced by the electrodynamic mechanism of diffraction and interference (Part II [5]) is seen superimposed with a quasi-perpendicular orientation on the long-wavelength NRPS at the boundary of the spot. By contrast to the effects produced beyond the spot boundary at 625 J/cm^2, the changes observed at 75 J/cm^2 outside the spot were negligible (Fig. 4c).

It is possible that in some areas of the enamel, the melting of the prisms' heads and their fusion produced inside the spot by three laser pulses summing up 75 J/cm^2 (Fig. 4c) was stronger than outside the spot after 25 pulses of 625 J/cm^2 (Fig. 4a). On the other hand, on other areas of the same upper incisor irradiated with 75 J/cm^2 the ablation pattern inside the spot (Fig. 3) was similar to the calcination pattern produced outside the spot at 625 J/cm^2 on the lower molar (Fig. 4a). However, the packing of perpendicular prisms was different in the two teeth (Part I [4]). The question remains open whether or not at 625 J/cm^2 the surface density of absorbed energy outside the spot was higher, lower or similar to the corresponding value in the spot at 75 J/cm^2 fluence, whatever the mechanisms of (indirect) heating beyond the boundaries of the spot. The question of the calcination halo beyond the spot requires further experimental and theoretical studies.

The fact that the laser induced effects outside the spot are appreciably less important than inside both at 75 and at 625 J/cm^2 suggests that they are induced by thermal radiation from the plasma plume or by the oscillating electric field around the spot [33], in contrast to the strong heating-associated effects inside the spot which are due significantly to the direct laser radiation. It is most plausible that these peripheric effects at the origin of calcination halo and its fissures decrease outside the spot with the distance, for instance like $\exp(-\alpha R)$ [33] or like $1/R^2$. Further research is needed for a better understanding of detrimental effects beyond the spot boundary and for optimizing appropriate parameters of the laser irradiation (pulse duration, energy per pulse, fluence, frequency, etc.).

Time evolution of laser pulse, plasma formation and heat diffusion

Let apart the small fraction of radiation scattered inward and absorbed subsequently in the enamel, the radiation absorbed directly in the spot is converted into heat and transferred to cooler

regions by conduction, which depends upon the dental tissue's thermal conductivity and diffusivity. Diffusion time, or time constant of a thermal response, is typically defined as [45]:

$$\tau_T = \frac{\delta^2}{4\kappa} \tag{14}$$

where κ is thermal diffusivity and δ a characteristic length. Because the penetration depth is very shallow with respect to the spot diameter, the characteristic length will equal the penetration depth, $\delta = d = 1/\mu_a = (20 – 40)$ μm (Part II [5]) and heat will be mainly conducted downward. A thermal relaxation time τ of 25 μs was estimated for λ = 9.6 μm for compact bone [26]. Assuming that enamel at 10.6 μm has a penetration depth close to the bone at 9.6 μm, the same order of magnitude is plausible for the thermal response time of enamel, $\tau \sim 25$ μs. This value is much larger than the laser duration τ_L and the plasma formation time τ_P,

$$\tau_T = 25\ \mu s >> 2\ \mu s = \tau_L \tag{15}$$

$$\tau_T = 25\ \mu s >> 150\ ns = \tau_P\ . \tag{16}$$

It follows that the heat transfer by downward diffusion – and even more by radial conduction – is slow as compared to the radiative laser action and to the plasma time constant, and probably contributes less to the thermo-mechanical ablation during the laser pulse. Although downward and radial heat diffusion immediately after the end of the laser pulse can take place and may contribute to the calcination observed beyond the boundary of the spot (Fig. 4a), it is probable that the radiative heat transfer from the plasma or by other mechanisms plays the major role in this effect. One possible mechanism can involve the exponential (as contrasted to abrupt) decrease outside the border of the oscillating electromagnetic field produced inside the laser spot [33]. This view is supported by the large fissures observed around ~300 μm (and probably also present beyond the enamel area intercepted in the SEM image from Fig. 4a), which are plausibly due to fast contraction of the enamel by the rapid cooling. After heating by radiation, the temperature drops appreciably faster than the time required for the heat to reach a large distance by radial diffusion. A related effect observed in enamel by us (Part I [4]) and by another group [62] was the formation of a halo of around the spot, discussed above. Radiative heat transfer from plasma formed in the vapor plume but not heat diffusion from the spot was the mechanism postulated for the altered halo produced by laser in ceramics [64]. The above discussion also suggests that downward diffusion of heat in enamel overcomes radial diffusion.

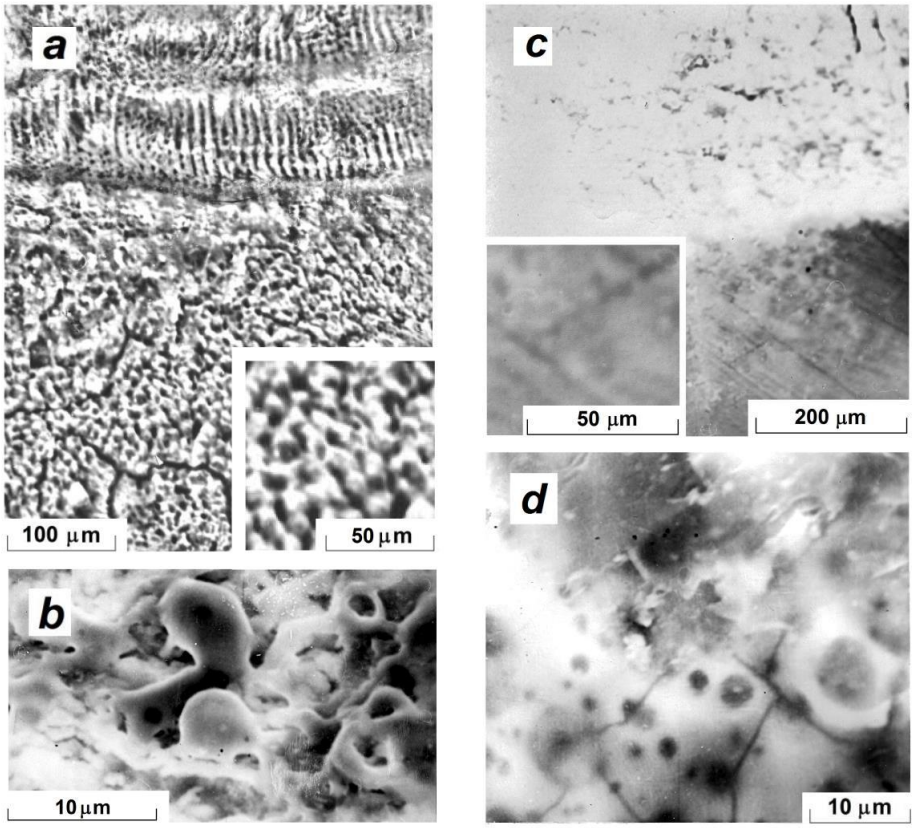

Fig. 4. Comparative laser irradiation effects on enamel outside and inside spot. (a) Calcination of enamel and superficial melting of prisms heads outside the laser spot (lower part) and resonant periodic structures inside the spot produced on the lower molar at 625 J/cm^2 fluence (upper part). (b) Higher magnification of melted enamel with boiling and irregular aspect inside the spot at 625 J/cm^2 fluence. (c) Lacking or negligible melted enamel outside the spot at 75 J/cm^2 (lower part) and incipient morphologic changes inside the spot produced on the upper incisor at 75 J/cm^2 (upper part). (d) Higher magnification display of melted enamel with smooth and glassy aspect inside the spot at 75 J/cm^2 fluence. The prisms were perpendicular in both enamel samples, but in (a, b) the prisms were sharply laid off with interprism spaces, while in (c, d) they were poorly expressed

Thermal ablation depth

The thermal ablation depth produced in enamel by each ~2 μs single pulse of the TEA-CO_2 laser 10.6 μm source at 25 J/cm^2 nominal fluence, and assuming an ablation fluence threshold of 13 J/cm^2 (Fig. 1 of Part II [5]), should be of the order of magnitude of a few μm as suggested by comparison to other laser ablation studies. For instance, we can refer to the effects of ultrashort 50 fs laser pulses generated by a Ti:Sapphire chirp modulation pulse amplifier system with a frequency-doubled, Nd:YAG pump laser. The corresponding ablation threshold is lowered to around 0.5 J/cm^2, and the ablation rate is about 1 μm/pulse at 3 J/cm^2 for enamel and dentin [24]. A Nd:YAG laser (λ = 1.064 μm) at fluencies of ~30 J/cm^2 and of ~70 J/cm^2 produced an ablation depth of ~4 μm in stainless steel and of ~3 μm in Al_2O_3 ceramics, respectively [64]. A comparison is reasonable because these materials have melting points of the same order of magnitude as enamel. The melting points of steel and alumina are of 1400 – 1800 and 2072 ^oC, respectively, while that of enamel is of 1280 ^oC, and that of altered compounds formed in enamel during the laser pulse heating is higher than 1600 ^oC [65 Kuroda]. (Unfortunately we do not have all data for the latent heat of fusion. Moreover hydroxyapatite, the major enamel compound, converts to β-tricalcium phosphate above 800^o C.) We may add that enamel has a ceramics-like structure. In brief, one can estimate a thermal ablation rate of 1 – 4 μm per pulse with the TEA-CO_2 laser at 25

J/cm^2 fluence. For 25 pulses, the depth of ablated spot could be estimated to about 25 – 100 μm. This is qualitatively confirmed by the observation of the very shallow depressions produced by laser in the enamel (Fig. 1A and 1C of Part I [4]). By contrast, the deep depression produced in cementum (Fig. 1B of Part I) is the result of a completely different process, namely hydrokinetic ablation, and was due to the residual water content in this porous tissue.

Suggestions for further studies

It was noted throughout Parts I–III of our study that due to the radial temperature gradient in the laser spot as evidenced in the ablation pattern gradient (Fig. 1C and 1D) and explained by our surface waves model, the crystallographic, chemical and elemental changes are expected to vary from the centre to the boundary. In addition to SEM and AFM, other surface micromapping and depth profiling analytical analysis methods may be used for the characterization of these position-dependent laser-induced changes. They may include elemental mapping using electron probe and proton microbeams as well as focused beams of synchrotron radiation. Such techniques yield valuable compositional and structural information [66] potentially relevant to the local changes induced by laser irradiation. Finally, because our capillary waves model underline the influence of enamel prisms orientation in the characteristics of wave-like patterns generated by laser irradiation, it would be useful to elaborate an *in situ* optical diagnosis method able to discriminate between dental enamel with perpendicular and parallel prisms [67].

Possible clinical developments

In the attempt to provide an unitary picture, this particular Section of our paper refer to the theoretical models and concepts as well as to their experimental support and clinical implications, as they are revealed both from the present Part III and from Part II altogether.

The discussion of the roughness vs. fluence relationship in Part II can be most relevant from the perspective of dental applications in therapy and prophylaxis. The two functions which fit the experimental data showed that a finite saturation roughness R_{max} should be *a priori* assumed as a prerequisite in the derivation of both the exponential saturation and the Langmuir function. This suggests that applying an indefinitely larger number of thermally isolated (i.e., at sufficiently low frequency) TEA-CO_2 laser pulses of ~2 μs, even above 625 J/cm^2 fluence, one could not expect to produce a monotonous increase in the roughening effects, at least on a scale of hundreds of nm. It appears that hydrokinetic ablation or probably much shorter laser pulses at high repetition rate could provide a more efficient control of the 'dental drill', without causing thermal damage of the pulp. Whilst this may limit the palette of dental therapy applications of μs-pulse IR lasers without water spraying, it also reveals the advantage of preventing undesired deep penetration in the hard dental tissue and pulp damage. It also reveals an advantage for caries prevention because only a relatively thin surface layer of enamel will be modified (ablated) by the pulsed 10.6 μm laser radiation. The roughness vs. fluence relationship confirms indirectly the fact that the TEA-CO_2 laser radiation at ~2 μs pulse duration and lower fluence (e.g. in the 13 – 75 J/cm^2 interval) could be more suitable for enhancing the resistance to incipient demineralization than higher fluence irradiation. Indeed, a gentle irradiation seals the enamel surface by superficial melting of prisms without roughening too much the melted material.

The surface alteration outside the spot is expected to produce opposite clinical effects: the limited melting of prisms' heads reduces the permeability of enamel and thus exhibits a protective action against caries formation, in contrast to the generation of large fissures which will facilitate the access of demineralizing organic acids in the deeper layers of enamel.

In the case of laser spots with Gaussian profile, the radial gradients of ultrastructural changes (at least those produced at 625 J/cm^2 fluence) may induce not only gradients of rugosity but also gradients of resistance to demineralization due to gradients of crystallographic, chemical and elemental changes. The present theoretical models, which take into account the large diameter of the spot (5 mm), may allow for a certain radial control on features of ultrastructural modifications of the enamel surface according to the distance from the center. Therefore, a degree of laser spots overlapping on the tooth surface should be produced according to the depth of

melted enamel layer at center and at the boundary and to the desired effect (roughening, caries prevention or caries treatment).

This overlapping could also prevent some boundary effects which may be not beneficial from the dental viewpoint. In the area outside the spot at 625 J/cm^2 fluence, calcination and relatively large fissures formation may stand for a possible detrimental effect of the μs-pulse TEA-CO_2 laser irradiation. Most probably they are generated by the radiative heating from the plasma plume in the melt expulsion regime. We suggested (Part I [4]) a possible use of this high fluence for the roughening of the enamel surface by periodic patterns and quasi-disordered bubbles formation in view of increasing the bond strengths of composites to enamel [68] and thus extending the lifetime 1) of dental restorations, as well as 2) of molar groves' sealings by fluid composite restoration materials aiming to protection against dental hypersensitivity. Some remedies are necessary in order to prevent undesired effects of possible large fissures produced around the laser spot. A simple suggestion, from the dental point of view, could be to shape the composite obturation so as to exceed the laser spot boundaries by a few tenths of millimeters and thus to seal the possible fissures which may form in the calcination area.

Conversely, at 75 J/cm^2 fluence, the changes observed outside the spot were negligible, with no calcinations, while inside the spot the prism heads were completely melted forming a compact mass of enamel with smooth and glassy morphology showing rare and narrow fissures only and covering completely the interprism spaces. At the same time physiognomic changes were minimal. This supports the recommendation of 75 J/cm^2 fluence of the TEA-CO_2 pulses for increasing the resistance of enamel against demineralization. To reduce the formation of narrow cracks by thermophysical effects, the theoretical discussion suggests new questions for further studies based on the relations between the laser pulse duration, the plasma formation time, and enamel's material constants.

The results suggest also that it may be reasonable to look after a certain fluence value where one could expect a reduction of the peripheral calcination effects without loosing completely the benefit of incipient melting of the prisms heads. However in dental applications the conjectured optimal value would be probably different for enamel with perpendicular and with parallel prisms, respectively.

As the theory shows that the total absorptivity of the target is larger when the electric field vector of a linearly polarized incident wave is directed along the longer side of the object [33], the possibility to use in future studies polarized laser radiation may help to take into account the anatomical shape and size of the tooth for optimizing the irradiation conditions.

One has to take into consideration also the formation of the plasma plume in relation with the oral cavity anatomy; the plume, extending in the air up to a few centimeters, as visible in our experiments, may present a risk of burning the soft tissues of the mouth. From this viewpoint, pulses of lower energy and a lower fluence might be preferable for practical dentistry.

In accordance to the experimental results, the theoretical models showed significant differences in the effects produced by the TEA-CO_2 laser irradiation on the enamel with perpendicular and parallel prisms. Moreover in our models specific relationships between the physical parameters of the ablation and the ultrastructural effects produced in enamel were established. This opens a new and prospective field in the experimental and clinical laser dental research. In long run, based on our results and on the study of the dependence of enamel surface's optical parameters on the prisms' orientation, the construction of devices adequate to non-invasive *in vivo* diagnosis of prism orientation should be necessary for reproducible clinical results of practical laser irradiation in the dental surgery.

3. Conclusions

The new theoretical developments presented in this part of our study were aimed to explain some remarkable characteristics of the ablation patterns produced in dental enamel by the pulsed TEA-CO_2, 2 μs-long, non-polarized, Gaussian laser beam at 625 J/cm^2 fluence. The physical picture was the following. The enamel was 'boiling' in the center of the spot, while 1)

concentric non-resonant periodic structures (NRPS) of ~42 and ~68 μm period in the enamel with perpendicular and parallel prisms, respectively, and 2) resonant periodic structures (RPS) of ~11 μm period in enamel with perpendicular prisms, were imprinted on target surface (discussed in Part II from the electrodynamical viewpoint). The ablation pattern suggests a strong radial temperature gradient associated with the Gaussian laser spot. The comparatively long ~2 μs laser pulse generates a melt expulsion domain, characterized by a very low plasma threshold. Plasma was produced with a high yield by colisional ionization in the vaporized substance, even at 1.25 x 10^7 W/cm^2 (5 J/pulse and spots of 5 mm diameter). Moreover, because the plasma formation time of ~150 ns was much shorter than the laser pulse duration of ~2 μs, the laser pulse was partially screened by the plasma. Thus, probably more than half of the incident energy is lost in the plasma.

However, part of the plasma energy was returned back to the enamel in the form of shock and acoustic waves, with a maximum intensity at the center of the spot. This was possibly involved in the concentric wave generation and in the splashing of molten enamel or flaked-of debris beyond the spot boundary. Another part of the returned plasma energy was involved in the radiative thermal damage of the enamel area outside the crater. We made an estimate of the shock wave pressure produced by the plasma and showed that it was inferior to the tensile strength of calcified tissues. Therefore, the shock wave did not disrupt directly the enamel, and the cracks and calcinations observed beyond the spot boundaries were assigned to radiative heating from plasma. The analysis of the time evolution of laser pulse, plasma formation and heat diffusion, showed that the contribution of the radiative heating from plasma to these clinically undesired effects. appears to be more important than downward and radial heat transfer during and after the laser pulse.

Here we proposed for the first time a simple physical model of surface and thermal capillary waves of the melted enamel layer, to explain the observed NRPS and their dependence on the prisms' orientation. The model is a first approximation which considers direct heat generation only, without plasma involvement. The basic postulate is that the SEM-observed frozen surface waves were generated by a sudden pressure build-up in the liquid phase produced by turbulent boiling, vaporization and ejection of the molten enamel at the center of the spot. Assuming the 'shallow water' regime for the surface waves of the melted enamel, the relative energy fluxes per unit of wave-crest length and the relative total power stored in the wave systems were evaluated and the ratio between the corresponding amounts helped understanding semiquantitatively the differences in the ablation patterns of enamel with perpendicular and parallel prisms (the NRPS 'waves' with periods of about 42 and 67 μm, respectively).

The results of the capillary wave model postulated in Part III were in agreement to the semiqualitative interpretation based upon the density of surface defects counted on SEM images of native enamel with perpendicular and parallel prisms. The model can be applied both to NRPS and RPS. Accordingly, the energy stored in the two NRPS wave systems of 42 and 68 μm was about the same or very close, irrespective of the prisms' orientation, although the resulting periodic patterns were different. However, the total energy stored in the wave systems was larger in the enamel with perpendicular prisms (42 μm NRPS plus 11 μm RPS) as compared to the one with parallel prisms (NRPS of 68 μm), in agreement with the larger surface density of defects in the enamel with perpendicular prisms. Complementarily, in the enamel with perpendicular prisms the longer wavelength (NRPS) mode of Λ = 42 μm could be assumed to be just a thermal capillary wave, just as the shorter wavelength (RPS) mode of Λ = 11 μm – that is, the surface was distorted only by thermal fluctuations in both cases. The two modes undergo equipartition and store a mean energy of $kT/2$ each. This result is in agreement with the physics of the melt expulsion regime which is characteristic for long duration laser pulses (~2 μs in our case).

The wave amplitude was roughly evaluated from the standard SEM images to 1.5 – 7.5 μm, and a depth of 5 – 10 μm was postulated for the liquid layer in the model. Nevertheless, for a precise measurement of the waves' height, special techniques such as 3D SEM secondary electron with tilting of specimen stage and use of glass beads as dimension standards should be used. However, a precise comparison to the model's predictions was not possible at this stage because only the ratios of various parameters were evaluated.

To understand other thermo-mechanical effects, the heat transfer during the laser pulse was analyzed *via* the evaluation of the diffusion time, or time constant of thermal response τ,

which depends on a characteristic length approximated as equal to the penetration depth, $\delta = d = 1/\mu_a \sim 20 – 40$ μm. Assuming $\tau \sim 25$ μs this estimation showed that heat will be conducted mainly downward, and that this downward heat diffusion – and even more the radial conduction – is slow as compared to the radiative laser action (~2 μs) and to the plasma time constant (~150 ns). The relations between the diffusion time, the laser pulse duration and the plasma formation time suggested that the possible contributions of the downward and radial heat diffusion to the calcination of enamel beyond the boundary of the spot are less important than the radiative energy transfer from the plasma or from the oscillating electric field outside the spot.

In view of new possible clinical applications, the theoretical approach supplemented the empirical results with a basis for a well-balanced selection of the working fluence values, according to prisms orientation and to radial dependence of effects. They permit a larger perspective for treatment optimization by extending the experimental conditions (e.g. with the use of polarized radiation, and of lasers with shorter pulse duration). For the dental practitioner, the aim of the optimization may be in particular the control of the surface roughening by the 'boiling' and by periodic ablation patterns in view of an improved adherence of restorative materials, as well as the reduction of enamel calcination outside the laser spot.

The theoretical discussion and the above models are intended to provide a deeper physical insight to the laser-enamel interactions, but also to open new prospects for coming research. Along with the experimental results presented in Part I, our theoretical approach of Parts II and III proved that the potential for TEA-CO_2 laser applications in hard tissues dentistry is far from being exhausted, and that a large field remains open on this ground for next studies.

Acknowledgement

The authors acknowledge with thanks the partial support of this work by UEFISCDI under the contract 19_RO-FR/2014. E.A.P. is grateful to Prof. Marian Apostol (Bucharest) for carefully reading the manuscript and valuable suggestions in the development of the theoretical models. The authors express their regrets for the disappearance of I. Patru, departed before the preparation of this article.

References

[1] R.A. Convissar, Principles and Practice of Laser Dentistry. Mosby Elsevier, St Louis, MO (2010)
[2] L.J. Miserendino, R.M. Pick (Editors), Lasers in Dentistry, Quintessence Publishing Co. Inc., Hanover Park, IL. (1995)
[3] A. Hussein, (Review), Archives of Orofacial Sciences **1**, 1 (2006)
[4] E.A. Preoteasa, Elena S. Preoteasa, I.N. Mihailescu, P. Lucuta, A. Moldovan. Digest J. Nanomater. Biostruct. **8**, 987 (2013) („Part I")
[5] E.A. Preoteasa, I.N. Mihailescu, Elena S. Preoteasa, Digest J. Nanomater. Biostruct. **9**, 1021 (2014), („Part II")
[6] M. Pao-Chang, X. Xion-Qui, Z. Hui, L. Zheng, Z. Rui-Peng, Laser Surg. Med. **1**, 375 (1981)
[7] R. Mullejans, G. Eyrich, W.H. Raab, M. Frentzen, Lasers Surg. Med. **30**, 331 (2002)
[8] M.M. Ivanenko, T. Mitra, P. Hering, Optical Biopsy and Tissue Optics, SPIE Proc. **4161-08**, 46 (2000)
[9] G. Sun, Dent. Clin. North Am. **44**, 831 (2000).
[10] P. Viraparia, J.M. White, R.M. Vaderhobli, In: CO2 Laser - Optimisation and Application, (D.C. Dumitras, editor) InTech, Rijeka (Croatia)-New York-Shanghai (2012)
[11] J.D. Featherstone, Dent. Clin. North Am. **44**, 955 (2000)
[12] S.M. McCormack, D. Fried, J.D.B. Featherstone, R.E. Glena, W. Seka, J. Dent. Res. **74**, 1702 (1995)
[13] J.D.B. Featherstone, N.A. Barrett-Vespone, D. Fried, Z. Kantorowitz, W. Seka, J. Dent. Res.

77, 1397 (1998)
[14] Z. Kantorowitz, J.D. Featherstone, D. Fried, J. Am. Dent. Assoc. **129**, 585 (1998)
[15] C.-Y.S. Hsu, T.H. Jordan, D.N. Dederich, J.S. Wefel, J. Dent. Res. **80**, 1797 (2001)
[16] K. Müller-Ramalho, C. de Paula Eduardo, N. Heussen, R. Garcia Rocha, F. Lampert, C. Apel, M. Esteves-Oliveira, Lasers Med. Sci. **28**, 71 (2013)
[17] X.-L. Gao, J.-S. Pan, C.-Y. Hsu. J. Dent. Res. **85**, 919 (2006)
[18] L. Stewart, G.L. Powell, S. Wright, Operative Dentistry **10**, 2 (1985)
[19] C.B. Gimbel, Dent. Clin. North Am., **44**, 931 (2000).
[20] H.A., Wigdor, J.T. Walsh Jr., J.D. Featherstone, S.R. Visuri, D. Fried, J.L. Waldvogel, Lasers Surg. Med. **16**, 103 (1995)
[21] M.H. Niemz, Laser-Tissue Interactions: Fundamentals and Applications, Springer-Verlag, Berlin Heidelberg New York (1996)
[22] A. Sagi, T. Segal, J. Dagan. Mathematical Biosciences **71**(1), 1 (1984).
[23] M. Jaunich, S. Raje, K. Kim, K. Mitra, Z. Guo, Int. J. Heat Mass Transfer **51**, 5511 (2008)
[24] J. Neev, J. Squier, in Applications of Ultrashort-Pulse Lasers in Medicine and Biology, (J. Neev, editor), SPIE Proc. **3255**, 105 (1998)
[25] M.H. Niemz. in Applications of Ultrashort-Pulse Lasers in Medicine and Biology, (Joseph Neev, Editor) SPIE Proc. **3255**, 84 (1998)
[26] M.M. Ivanenko, G. Eyrich, E. Bruder, P. Hering, Lasers Life Sci. **9**, 171 (2000)
[27] D. Găzdaru, C. Chilom, M.A. Călin, C. Geantă, A. Popescu, Romanian J. Biophys. **18**, 73 (2008)
[28] L.V. Zhigilei, A.M. Dongare, CMES **3**, 539 (2002)
[29] G. Macaveiu, ISRN Biomed. Engn., Article ID 464293, 8 p. (2013)
[30] M.E. Abadi, M.H. Miran Baygi, A. Mahloojifar, S. Moghimi, Iranian J. Electric. Electron. Engn. **1**, 23 (2005)
[31] M.A. Golshan, M.G. Tarei, M.A. Ansari, A. Amjadi, J. Lasers Med. Sci. **2**, 109 (2011)
[32] D.M. Zezell, P.A. Ana, T.M. Pereira, P.R. Correa, W. Velloso Jr., 227-246 in: Developments in Heat Transfer (M.A. Dos Santos Bernardes, editor), InTech, Rijeka, Croatia (2011)
[33] A.M. Prokhorov, V.I. Konov, I. Ursu, I.N. Mlhailescu, Laser Heating of Metals, Adam Hilger, Bristol-Philadelphia-New York (1990)
[34] M. Gantri, H. Trabelsi, E. Sediki, R. Ben Salah, J. Biophys. **2010**, Article ID 253763, 9 p. (2010)
[35] S.L. Jaques, S.A. Prahl, Laser Surg. Med. **6**, 494 (1987)
[36] A. Vila Verde, M.M.D. Ramos, A.M. Stoneham, Phys. Med. Biol. **52**, 2703 (2007)
[37] W. Schulz, U. Eppelt, R. Poprawe. (Review) J. Laser Applic. **25**(1), 012006 1 (2013)
[38] I. Ursu, I. Apostol, D. Barbulescu, V. Lupei, I.N. Mihailescu, A. Popa, A.M. Prokhorov, N. I. Chapliev, V.I. Konov, Proc. SPIE Int. Soc. Opt. Eng. **398**, 361 (1983)
[39] V.A. Danilychev, V.D. Zvorykin, I.V. Kholin, A.Yu. Chugunov, Sov. J. Quantum El. **10**, 1518 (1980)
[40] V.I. Konov, Yu.V. Lavrent'ev, Yu.I. Stepanov, N.I. Chapliev, A.V. Shirkov, Sov. J. Quantum El. **13**, 1128 (1983)
[41] M. Stoica, D. Craciun, I.N. Mihailescu, 136-151 in: Laser Research and Engineering (V. Vasiliu, editor), Central Institute of Physics, Bucharest-Magurele (1989);
[42] V.I. Bergel'son, A.P. Golub', I.V. Nemchinov, S.P. Popov, Sov. J. Quantum El. **3**, 288 (1974)
[43] J.C. Koo, J. Appl. Phys. **48**, 618 (1977)
[44] B. Payne, The role of chromophore on pulsed laser ablation of biological tissues. Thesis, Univ. Denver (1994)
[45] A.J. Welch, J.H. Torres, W.-F. Cheong, Texas Heart Inst. J. **16**, 141 (1989)
[46] C.T.E. Gordon Jr., J. Dent. Res. **45**, 372 (1966)
[47] A.G. Doukas, A.D. Zweig, J.K. Frisoli, R. Birngruber, T.F. Deutsch, Appl. Phys. **B53**, 237 (1991)
[48] J.P. Cummings, J.T. Walsh Jr., Appl. Optics **32**, 494 (1993)
[49] A.P. Alloncle, D. Dufresne, M. Autric, J. Physique IV, Coll. C4, Supp. 111, **4**, C4 (1994)
[50] M. Cutroneo, L. Torrisi, C. Scolaro, Laser applications in bio-medical field, Univ.Messina, Preprint (2012)

[51] J. Bonse, J. Krüger, S. Höhm, A. Rosenfeld, Femtosecond laser-induced periodic surface structures, J. Laser Appl., Vol. 24, No. 4, July 2012, 042006-[pp. 1-7]
[52] L.D. Landau, E.M. Lifshitz, Fluid Mechanics. Course of Theoretical Physics (2nd revised edition), Pergamon Press (1986)
[53] H. Lamb, Hydrodynamics (6th edition), Cambridge University Press (1994)
[54] J.B. Herbich, Handbook of Coastal Engineering, McGraw-Hill Professional (2000)
[55] G. Falkovich, Fluid Mechanics, A Short Course for Physicists, Cambridge University Press (2011)
[56] S. Safran, Statistical Thermodynamics of Surfaces, Interfaces and Membranes, Addison-Wesley (1994)
[57] J.S. Rowlinson, B. Widom, Molecular Theory of Capillarity, Clarendon, Oxford (2002)
[58] I. Prigogine, From Being to Becoming, Freeman, San Francisco (1980)
[59] I. Ursu, I.A. Dorobantu, I.N. Mihailescu, M. Vlad, F. Spineanu, A.M. Prokhorov, V.I. Konov, V.N. Tokarev, Optics Lett. **14**, 853 (1989)
[60] J.C. Russ, Fractal Surfaces, Springer-Verlag, Berlin-Heidelberg-New York (1994)
[61] D.W. Zeng, K.C. Yung, Appl. Surface Sci. **180**, 280 (2001)
[62] M.K. Yamada, M. Uo, S. Ohkawa, T. Akasaka, F. Watari, Mater. Transact. **45**, 1033 (2004)
[63] R.H. Stern, J. Vahl, R.F. Sognnaes, J. Dent. Res. **51**, 455 (1972)
[64] S.V. Garnov, V.I. Konov, T. Kononenko, V.P. Pashinin, M.N. Sinyavsky, Laser Phys. **14**, 910 (2004)
[65] S. Kuroda, B.O. Fowler, Calcif. Tissue Int. **36**, 361 (1984)
[66] Eugen A. Preoteasa, Elena S. Preoteasa, Ioana Suciu, Atomic and Nuclear Surface Analysis Methods: A Novel Perspective for the Characterization of Dental Composites, Nova Science Publishers, Inc., New York (2012)
[67] G. Duplain, R. Boulay, P.A. Bélanger, Appl. Optics **26**, 4447 (1987)
[68] B. Ersu, B. Yuzugullu, A. Ruya Yazici, S. Canay, J. Dent. **37**, 848 (2009)